AFRL-ML-WP-TP-2006-503

PRECIPITATION IN Al-Zn-Mg-Cu ALLOYS MODIFIED WITH Sc AND Zr DURING AGING (Preprint)

M.R. Shaghiev, S.V. Senkova, and O.N. Senkov

DECEMBER 2006

This is a Small Business Innovation Research (SBIR) Paper.

Approved for public release; distribution is unlimited.

STINFO COPY

MATERIALS AND MANUFACTURING DIRECTORATE
AIR FORCE RESEARCH LABORATORY
AIR FORCE MATERIEL COMMAND
WRIGHT-PATTERSON AIR FORCE BASE, OH 45433-7750

REPORT DOCUMENTATION PAGE

Form Approved
OMB No. 0704-0188

1. REPORT DATE *(DD-MM-YY)*	2. REPORT TYPE	3. DATES COVERED *(From - To)*
December 2006	Journal Article Preprint	

4. TITLE AND SUBTITLE
PRECIPITATION IN Al-Zn-Mg-Cu ALLOYS MODIFIED WITH Sc AND Zr DURING AGING (Preprint)

5a. CONTRACT NUMBER
F04611-02-C-0014

5b. GRANT NUMBER

5c. PROGRAM ELEMENT NUMBER
62102F

6. AUTHOR(S)
M.R. Shaghiev, S.V. Senkova, and O.N. Senkov

5d. PROJECT NUMBER
2311

5e. TASK NUMBER
00

5f. WORK UNIT NUMBER
23110002

7. PERFORMING ORGANIZATION NAME(S) AND ADDRESS(ES)

UES, Inc.
4401 Dayton-Xenia Road
Dayton, OH 45432

8. PERFORMING ORGANIZATION REPORT NUMBER

9. SPONSORING/MONITORING AGENCY NAME(S) AND ADDRESS(ES)

Materials and Manufacturing Directorate
Air Force Research Laboratory
Air Force Materiel Command
Wright-Patterson AFB, OH 45433-7750

10. SPONSORING/MONITORING AGENCY ACRONYM(S)
AFRL-ML-WP

11. SPONSORING/MONITORING AGENCY REPORT NUMBER(S)
AFRL-ML-WP-TP-2006-503

12. DISTRIBUTION/AVAILABILITY STATEMENT
Approved for public release; distribution is unlimited.

13. SUPPLEMENTARY NOTES
This is a Small Business Innovation Research (SBIR) Paper. Submitted for publication in the Proceedings of Materials Science & Technology 2006 Conference and Exhibition (MS&T '06), publisher: MS&T Organizers. PAO Case Number: AFRL/WS 06-1953, 14 August 2006.

14. ABSTRACT
This paper was developed under a SBIR contract.
The effect of Sc additions on precipitation strengthening in AI-Zn-Mg-Cu alloys was studied after natural and artificial aging. Phase analysis was performed using transmission electron microscopy and computer simulations. Microhardness of the alloys was studied after different steps of aging and the strengthening mechanisms were discussed. It was found that Sc does not affect the kinetics of aging at room temperature, which is controlled by formation and growth of GPI zones. Sc also does not affect the kinetics of aging at 150°C, which is controlled by formation and growth of η' and η particles. However, the additions of Sc accelerate the aging process at l20°C within a period of time of formation and growth of GPII zones. It is concluded that the presence of Sc accelerates formation and growth of GPII zones in the Al-Zn-Mg-Cu alloys during artificial aging.

15. SUBJECT TERMS

SBIR, Al-Zn-Mg-Cu alloys, microhardness, natural aging, artificial aging, precipitation,

16. SECURITY CLASSIFICATION OF:			17. LIMITATION OF ABSTRACT:	18. NUMBER OF PAGES	19a. NAME OF RESPONSIBLE PERSON (Monitor)
a. REPORT	b. ABSTRACT	c. THIS PAGE			Daniel B. Miracle
Unclassified	Unclassified	Unclassified	SAR	16	19b. TELEPHONE NUMBER *(Include Area Code)* (937) 255-1305

Standard Form 298 (Rev. 8-98)
Prescribed by ANSI Std. Z39-18

Precipitation in Al-Zn-Mg-Cu Alloys Modified with Sc and Zr During Aging

M.R. Shaghiev, S.V. Senkova, O.N. Senkov

UES, Inc., 4401 Dayton-Xenia Rd., Dayton, OH 45432-1894, USA

Keywords: Al-Zn-Mg-Cu alloys, microhardness, natural aging, artificial aging, precipitation

Abstract

The effect of Sc additions on precipitation strengthening in Al-Zn-Mg-Cu alloys was studied after natural and artificial aging. Phase analysis was performed using transmission electron microscopy and computer simulations. Microhardness of the alloys was studied after different steps of aging and the strengthening mechanisms were discussed. It was found that Sc does not affect the kinetics of aging at room temperature, which is controlled by formation and growth of GPI zones. Sc also does not affect the kinetics of aging at 150°C, which is controlled by formation and growth of η′ and η particles. However, the additions of Sc accelerate the aging process at 120°C within a period of time of formation and growth of GPII zones. It is concluded that the presence of Sc accelerates formation and growth of GPII zones in the Al-Zn-Mg-Cu alloys during artificial aging.

Introduction

Aerospace industry has a substantial interest to the newer materials with high specific properties and low cost. Al-Zn-Mg-Cu 7000 series alloys have the highest strength among all commercial aluminum alloys [1]. Their strength is mainly controlled by precipitation reactions accompanying heat treatment. For this reason, precipitation from a solid solution is being one of the most extensively investigated areas of physical metallurgy of aluminum alloys [2-7]. Precipitation sequence in 7000 series alloys can be summarized as [2-4]:

Solid Solution → Guinier-Preston (GP) Zones → Metastable η′ → Stable η ($MgZn_2$)

The GPII zones and metastable η′ phase are believed to be responsible for peak hardening of these alloys, while transformation of η′ into stable η leads to a decrease in hardness (i.e. overaging) [4-5]. The effect of small additions of Sc and Zr on mechanical properties of advanced aluminum alloys has been studied extensively [2,8-12]. It was found that these elements can provide a superior combination of high strength and acceptable ductility [9-12]. Increased strength and improved ductility were related to the formation of fine coherent $Al_3(Sc,Zr)$ particles and refined grain structure. At the same time only limited and contradictory information is currently available on the effect of Sc on aging kinetics of Al-Zn-Mg-Cu alloys [12]. Therefore, the goal of the present work was to study the effect of Sc on the kinetics of precipitation and strengthening in Al-Zn-Mg-Cu alloys during natural and artificial aging.

Experimental

Two Al-Zn-Mg-Cu alloys produced by direct chill (DC) casting in the shape of 76 mm diameter rods, with the same nominal composition but different Sc concentrations of 0 and 0.38 wt. % Sc, were used as starting materials. These alloys were developed by UES, Inc. on request of the US Air Force for use at ambient and cryogenic temperatures [13,14]. The chemical compositions of the produced alloys are given in Table I.

Table I. Compositions (in wt.%) of the alloys studied in the present work

Alloy	Zn	Mg	Cu	Mn	Zr	Sc	Others	Al
SSA000	7.1	2.30	1.61	0.27	0.17	0	up to 0.3	Balance
SSA038	7.1	2.14	1.56	0.25	0.17	0.38	up to 0.3	Balance

The Vickers microhardness at 500 g load was measured in the regions of the flat polished surfaces of the transverse cross-sections, which were located about 15-20 mm from the center of the DC cast rods. The cast alloys were heat treated in air using resistance heated box furnaces with forced air convection. Homogenization of the alloys was performed at 460°C for 48 hours. TEM samples were subjected to additional two-step solution heat treatment at 460°C for 2 hours and 480°C for 1 hour with subsequent water quenching. For natural aging the samples were held at room temperature for different time periods. Artificial aging was performed at two different temperatures, 120°C and 150°C, with different soaking times and subsequent air cooling. Microstructural and phase analyses were conducted using a transmission electron microscope (TEM) Phillips CM200 operating at an accelerating voltage of 200 kV. Thin foils for TEM were twin-jet electropolished in a solution consisting of 20% HNO_3 and 80% methanol at -30°C. Experimental selective area diffraction patterns (SADP) were compared with the literature data [3-7,15] and corresponding SADPs simulated by Desktop Microscopist DM2.2Net software.

Results and Discussion

Effect of Sc on Microhardness after Natural and Artificial Aging

Dependencies of the Vickers microhardness of SSA000 and SSA038 alloys on the natural aging time are given in Figure 1a. The microhardness of both alloys increases logarithmically with an increase in the aging time, due to formation and growth of GPI zones (see below). On the initial stage of natural aging (during first 30 minutes after water quenching), the microhardness increases slowly indicating incubation period of the GPI zone nucleation. A rapid increase in microhardness is observed during natural aging within 30 minutes to 600 hours. At longer aging times, the rate of microhardness increase slows down, probably due to a decrease in the nucleation rate and the precipitate coarsening at a near saturated volume fraction of the GPI zones. The Sc-containing alloy has microhardness, which is about 120 MPa higher than that of the Sc-free alloy. This difference in the microhardness does not depend on the natural aging time, indicating that there is no effect of Sc on precipitation and growth of GPI zones.

Figure 1b shows microhardness of SSA000 and SSA038 alloys after artificial aging at 120°C for a different period of time. For both alloys, microhardness first increases with the aging time, reaches a maximum of about 2 GPa after 162-hour aging and then rapidly decreases. Within ~8 hours of aging microhardness increases slightly faster in the Sc-modified alloy, so that after 8 hours of aging at 120°C microhardness of SSA038 alloy is about 200 MPa higher than that of SSA000 alloy. However, at longer aging times the rate of the microhardness increase slows down in SSA038, while it almost does not

change in SSA000, resulting in near the same microhardness in these two alloys in the peak aged condition (after 162 h aging). After peak aging, the microhardness of both alloys decreases and has nearly the same values.

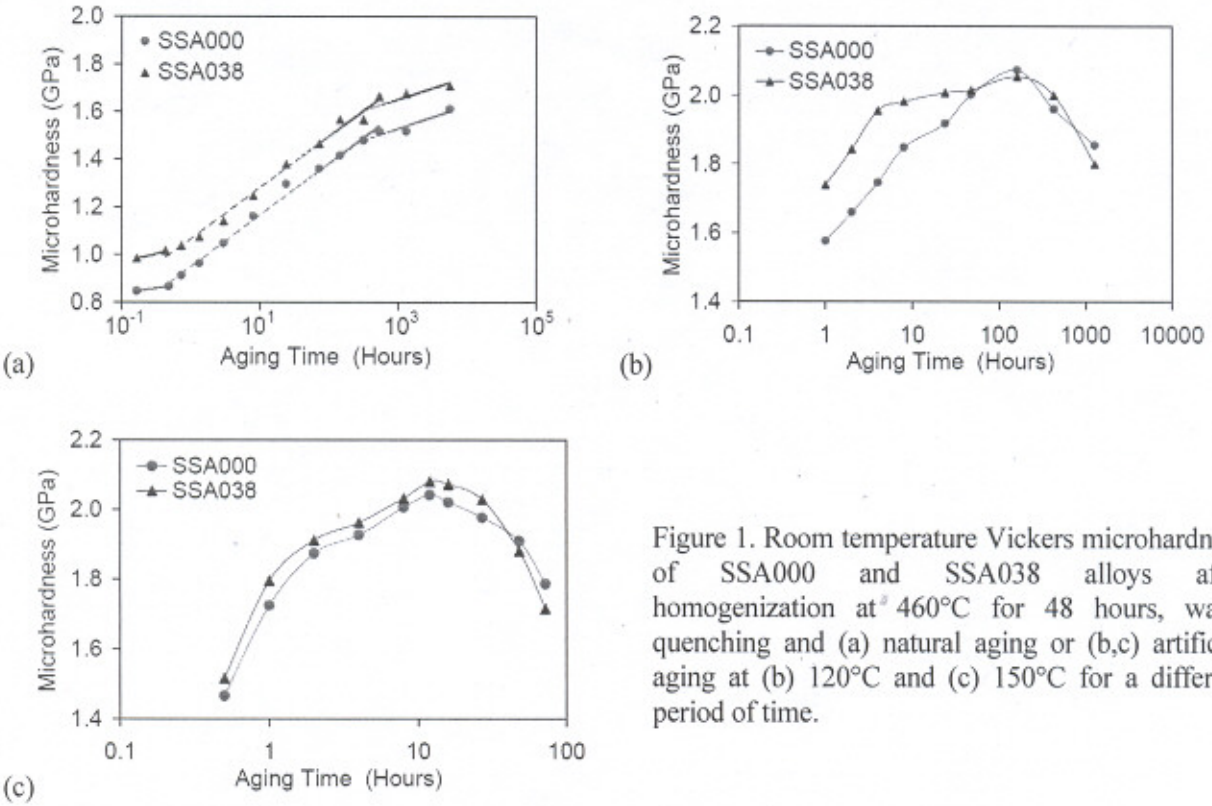

Figure 1. Room temperature Vickers microhardness of SSA000 and SSA038 alloys after homogenization at 460°C for 48 hours, water quenching and (a) natural aging or (b,c) artificial aging at (b) 120°C and (c) 150°C for a different period of time.

Dependencies of the Vickers microhardness of SSA000 and SSA038 alloys on the aging time at 150°C are given in Figure 1c. Unlike to artificial aging at 120°C, there is no substantial effect of Sc on the aging kinetics at 150°C, and an increase in the microhardness due to the presence of Sc almost does not depend on the aging time, Figure 1c. The difference in the microhardness of these alloys after aging at 150°C is about 80 MPa at any aging time. The peak microhardness in the alloys aged at 150°C was observed after shorter aging times, at about 12 hours.

Effect of Sc on Precipitation During Natural and Artificial Aging

Figure 2 represents simulated selected area diffraction patterns of studied alloys with different possible precipitation phases in $\langle 001 \rangle_{Al}$ and $\langle 112 \rangle_{Al}$ projections. Positions of diffraction spots from GPI and GPII zones are taken from the literature data [3,4,6,15], while diffraction patterns of the $L1_2$ [Al_3Zr or $Al_3(Sc,Zr)$], η' and η phases are simulated using Desktop Microscopist DM2.2Net software. Diffraction features of GPI zones are best viewed in the $\langle 001 \rangle_{Al}$ SADP, Figure 2a. In this SADP, main strong diffraction spots come from the aluminum matrix. Weak sharp diffraction spots at {h,k,l}={(2n+1),0,0}, {0,(2n+1),0} and {(2n+1),(2n+1),0} positions in the Al reciprocal lattice are from the $L1_2$ phase. The rows of diffuse spots at {1,(2n+1)/4,0} positions are from GPI zones. According to [3], the strongest diffuse spots from GPI are located at positions $\{1,1/4,0\}_{Al}$ and $\{1,7/4,0\}_{Al}$. According to [6], GPII zones can also be identified in $\langle 001 \rangle_{Al}$ projections as weak spots near $2/3\{220\}_{Al}$ positions, however, other work [15] indicates that diffraction features of GPII zones are not visible in this projection. According to [4], weak diffraction spots at $1/3\{220\}_{Al}$ and $2/3\{220\}_{Al}$ positions in

the $\langle 001 \rangle_{Al}$ SADP are from metastable η′ precipitates. Results of our simulations also show that only GPI zones and $Al_3Zr/Al_3(Sc,Zr)$ can be clearly identified in the $\langle 001 \rangle_{Al}$ SADP while diffraction spots from GPII zones, η′ and η phases are overlapping (see Figure 2a).

Another characteristic diffraction pattern for precipitation analysis is the $\langle 112 \rangle_{Al}$ SADP, Figure 2b. GPI have been shown to produce diffusive diffraction spots at $1/3\{311\}_{Al}$ and $2/3\{311\}_{Al}$ and GPII produce diffusive spots near $1/2\{311\}_{Al}$ [4]. Diffraction features of the η′ phase can also be observed in the $<112>_{Al}$ projections as diffraction streaks along $\{111\}_{Al}$ at 1/3 and 2/3 $\{220\}_{Al}$ positions [4], Figure 2b. As it is shown in Figure 2b, elongated spots slightly outside of $\{220\}_{Al}$ and $\{311\}_{Al}$, as well as near $\{111\}_{Al}$ and $\{222\}_{Al}$ positions, in the $\langle 112 \rangle_{Al}$ SADP (Figure 2b) indicate the presence of the equilibrium η phase. According to our simulations, diffraction spots from the $L1_2$, η′ and η phases, as well as from GPI and GPII zones, can be separated in the $\langle 112 \rangle_{Al}$ SADP. Therefore, the $<001>_{Al}$ and $<112>_{Al}$ SADPs were used to analyze precipitates present in the alloys after different aging conditions.

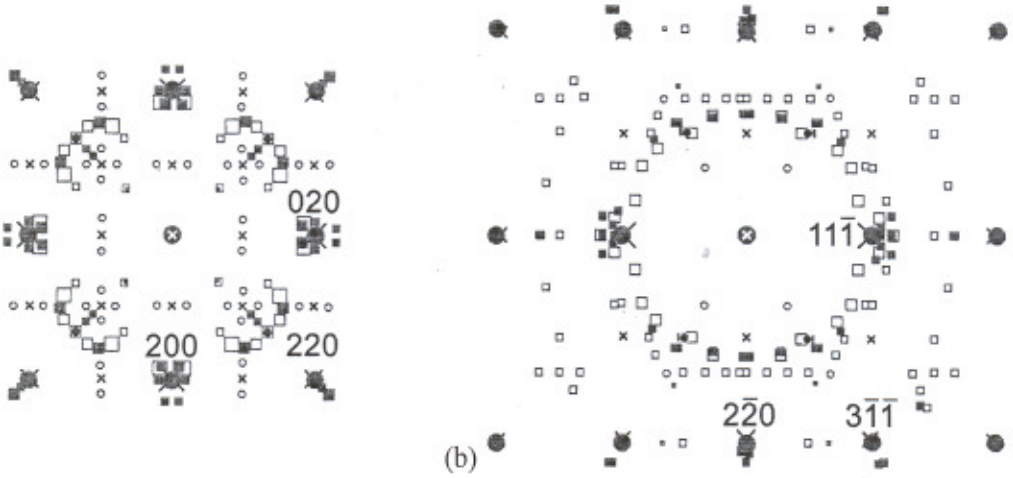

Figure 2. Simulated selected area diffraction patterns in (a) $\langle 001 \rangle_{Al}$ projection and (b) $\langle 112 \rangle_{Al}$ projection. Large filled circles are from fcc Al; crosses are from $L1_2$ phase; open circles are from GPI zones; small filled circles are from GPII zones; open squares are from η′ phase and filled squares are from η phase.

Typical dark field images of different precipitates observed in the present study are given in Figure 3. After solution treatment, water quenching and natural aging, fine Al_3Zr and $Al_3(Sc,Zr)$ particles are easily identified in, respectively, Sc-free and Sc-containing alloys (see Figures 3a and 3b). The average size of the Al_3Zr particles is about 15 nm and their number density is approximately $5x10^{14}$ cm^{-3}. The size of the $Al_3(Sc,Zr)$ particles varies from 5 nm to 40 nm, with an average size of about 22 nm, and their number density is about $1x10^{15}$ to $3x10^{15}$ cm^{-3}. The higher number density of the $Al_3(Sc,Zr)$ particles than of Al_3Zr particles is evidently responsible for the increased microhardness of the Sc modified alloy SSA038 in the solution treated and naturally aged conditions. The $Al_3(Sc,Zr)$ and Al_3Zr particles were present after all aging conditions studied in the current work and their size and number density did not change with aging time. Therefore, the diffraction features from these particles are not discussed in the following text.

Figures 3c and 3d show dark field images of, respectively, η′ and η particles after artificial aging at 150°C. After 1-hour aging at this temperature, the η′ phase particles have the average size of 2-3 nm and the number density of 10^{17}-10^{18} cm^{-2}, Figure 3c. After 12 hour aging at 150°C, the average η′ phase particle size increases to ~5-6 nm and larger η phase particles with the average size of 9-11 nm and the number density of ~ 10^{15}-10^{16} cm^{-2} can also be identified (see Figure 3d).

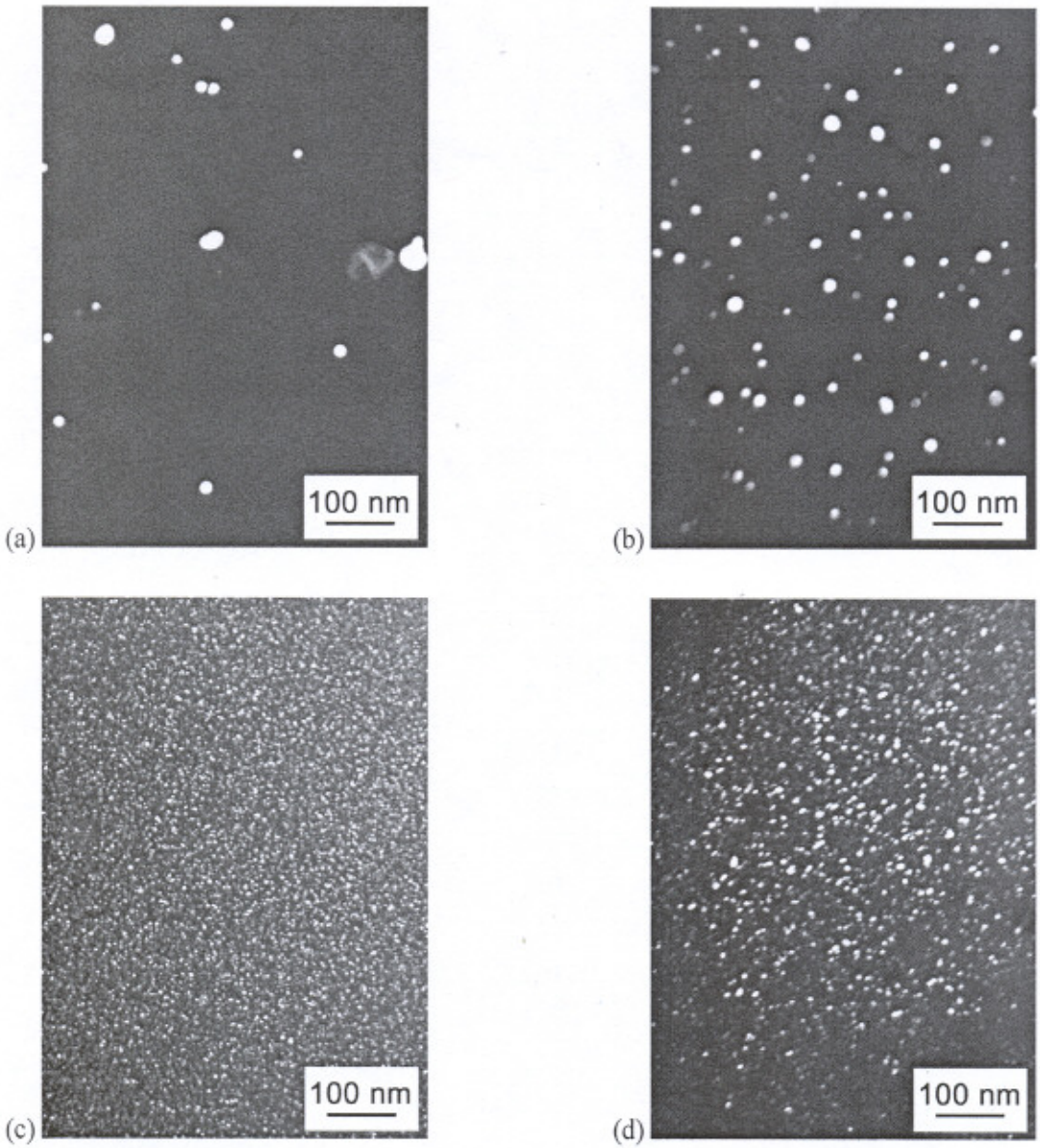

Figure 3. Typical dark field images in (a) Al_3Zr; (b) $Al_3(Sc,Zr)$; (c) η' and (d) η phase diffraction spots. (a) SSA000 and (b) SSA038 alloys after natural aging; (c) SSA000 after aging at 150°C for 1 h; (d) SSA038 after aging at 150°C for 12 h.

Figures 4 and 5 show SADPs in $\langle 001 \rangle_{Al}$ and $\langle 112 \rangle_{Al}$ projections from SSA000 and SSA038 alloy samples naturally aged for ~1000 hours. Characteristic patterns of diffuse spots associated with GPI zones are observed in both SSA000 and SSA038 alloys. No diffraction features of GPII zones or η' particles are found in the naturally aged samples. This result reveals that an increase in the microhardness during natural aging of these alloys is due to precipitation and growth of GPI zones. The fact that the kinetics of the natural aging is the same in both Sc-containing and Sc-free alloys (see Figure 1a) indicates that Sc does not have any effect on formation and growth of the GPI zones in the Al-Zn-Mg-Cu alloys.

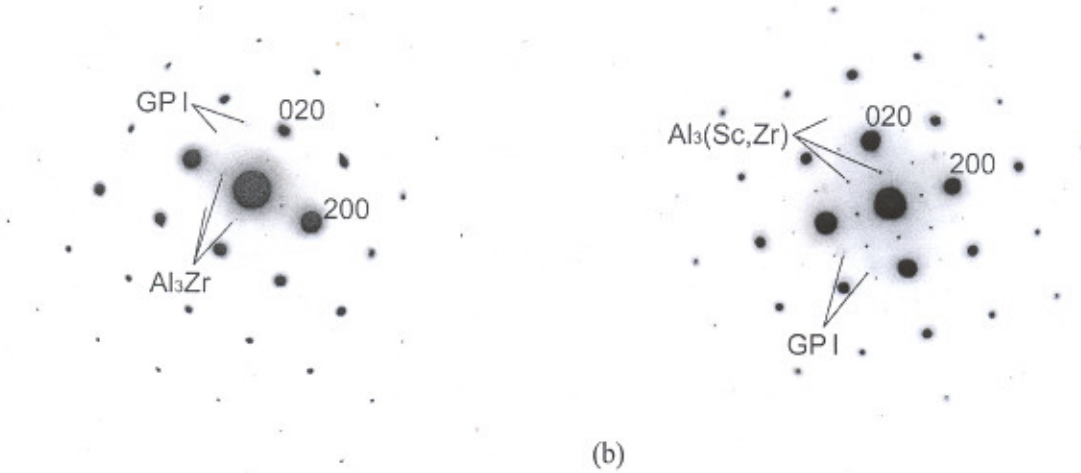

(a) (b)

Figure 4. Selected area diffraction patterns in $\langle 001 \rangle_{Al}$ projection of (a) SSA000 and (b) SSA038 alloy samples after solution annealing, water quenching and subsequent natural aging for ~1000 hours.

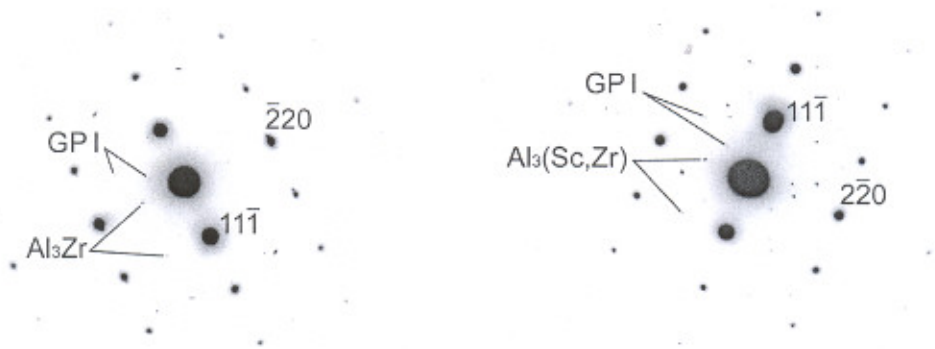

(a) (b)

Figure 5. Selected area diffraction patterns in $\langle 112 \rangle_{Al}$ projection of (a) SSA000 and (b) SSA038 alloy samples after solution annealing, water quenching and subsequent natural aging for ~1000 hours.

Typical SADPs of the samples after solution annealing, water quenching and subsequent artificial aging at 120°C for 24 hours are given in Figure 6. The diffraction analysis reveals the presence of GPI and GPII zones as major precipitates in the Sc-free alloy, Figure 6a. There are also some diffraction features indicating that η' particles started to form in SSA000 at this aging condition. On the other hand, in the Sc containing alloy GPII zones and η' particles prevail after aging at 120°C for 24 hours, Figure 6b. Weak diffraction spots at $2/3\{311\}_{Al}$ positions indicate that some GPI zones are still present in SSA038 alloy; however, their intensity is much weaker than in the Sc-free sample. The results of the SADP analysis allow us to suggest that formation and growth of the GPII zones during artificial aging at 120°C occur faster in the Sc-containing alloy leading to earlier formation of the η' particles. The accelerating formation and growth of GPII zones may result from a higher number density of vacancy-rich clusters (VRC) [18,19] in the Sc-containing alloy. GPII zones are believed to nucleate on VRC [19]. Indeed, it has been recently shown [20] that the binding energy of a Sc atom with a vacancy is about 0.35 eV,

which is higher than that for other solutes. Therefore, higher number density of VRC should be expected in the Sc-containing alloy than in the Sc-free alloy after solution treatment and water quenching. This different kinetics of formation and growth of GPII zones in the Sc-free and Sc-containing alloys explains a more rapid increase in the microhardness at earlier stages of aging at 120°C in the Sc-containing alloy.

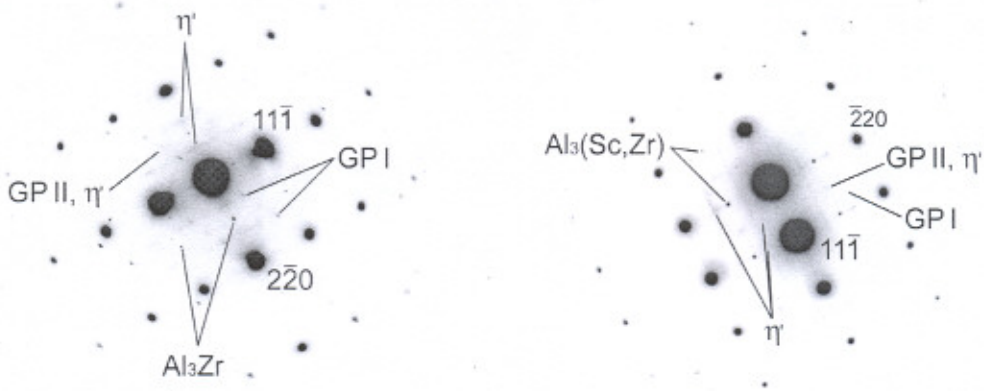

(a) (b)

Figure 6. Selected area diffraction patterns of (a) SSA000 and (b) SSA038 alloy samples after solution annealing, water quenching and subsequent artificial aging at 120°C for 24 hours in $\langle 112 \rangle_{Al}$ projection.

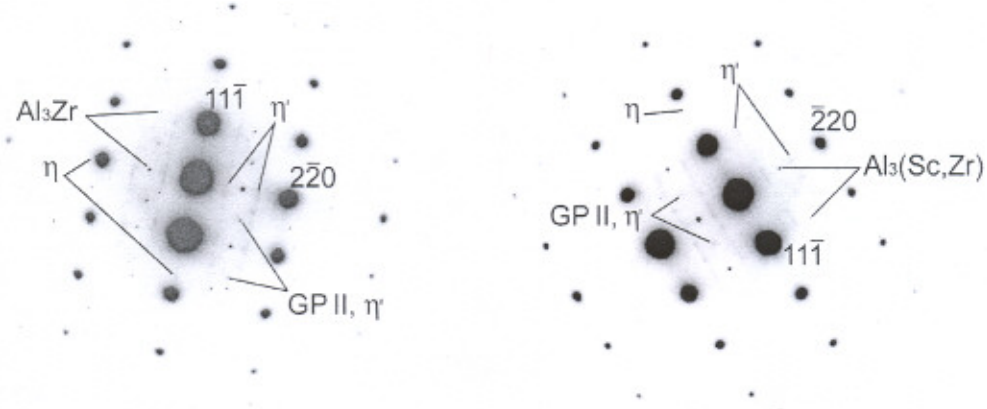

(a) (b)

Figure 7. Selected area diffraction patterns of (a) SSA000 and (b) SSA038 alloy samples after solution annealing, water quenching and subsequent artificial aging at 120°C for 162 hours in $\langle 112 \rangle_{Al}$ projection.

Figure 7 shows typical SADPs of SSA000 and SSA038 alloys after aging at 120°C for 162 hours, which corresponds to the peak aging condition (see Figure 1b). No diffraction spots from GPI zones are detected indicating that the GPI zones were completely dissolved. On the other hand, diffraction features of GPII zones and η′ particles are observed in both alloys. Besides, weak diffraction spots near $\{220\}_{Al}$ and $\{222\}_{Al}$ indicate that the η phase starts to form. The presence of the equilibrium η phase suggests that the maximum size of the metastable η′ phase particles in this aged condition reached its critical

value providing the peak hardening [16]. Almost the same values of microhardness in the Sc-containing and Sc-free alloys after 162-hour aging at 120°C can be due to coarser particles (both η′ and η) and higher volume fraction of the equilibrium η phase in the Sc-containing alloy. The hardness loss associated with the larger particle size leads to an apparent decrease in the hardening effect from the $Al_3(Sc,Zr)$ particles. Similar conclusion has been made earlier [17].

Typical SADPs of SSA000 and SSA038 alloys after solution annealing, water quenching and subsequent aging at 150°C for 1 hour are given in Figure 8. The η′ particles are found to be the major precipitates in this aging condition in both alloys. Diffraction spots from the η phase are not observed. However, the diffraction features of both metastable η′ and equilibrium η phases are identified on the SADPs in both the alloys in the peak aged condition, i.e. after 12 hours at 150°C, Figure 9. The latter suggests that the metastable η′ phase reaches its maximum volume fraction providing the highest microhardness of the alloys and starts to transform into the equilibrium η phase.

(a) (b)

Figure 8. Selected area diffraction patterns of (a) SSA000 and (b) SSA038 alloy samples after solution annealing, water quenching and subsequent artificial aging at 150°C for 1 hour in $\langle 112 \rangle_{Al}$ projection.

After 48-hour aging at 150°C the major precipitates in both SSA000 and SSA038 alloys remain the same: η′ and η particles, Figure 10. At the same time, diffraction spots from the η phase become stronger suggesting that the volume fraction of the η precipitates increases significantly. Besides, diffusive streaks along $\{111\}_{Al}$ from the η′ phase are rather thick and discrete, which indicates coarsening of the η′ phase particles. The mean size of the η′ particles after aging at 150°C for 48 hours is 6-7 nm and the size of η precipitates is about 11 nm in both SSA000 and SSA038 alloys. Coarsening of the major hardening precipitates, η′ phase particles, as well as an increase in the volume fraction of the rather coarse η phase particles, seems to be responsible for a decrease in microhardness in the overaged condition. Similar character of precipitation after aging at 150°C resulted in essentially the same microhardness values in both Sc-containing and Sc-free alloys (see Figure 1c). Unlike to aging at 120°C, no effect of Sc on the precipitation kinetics during artificial aging at 150°C was found, in agreement with the microhardness measurements.

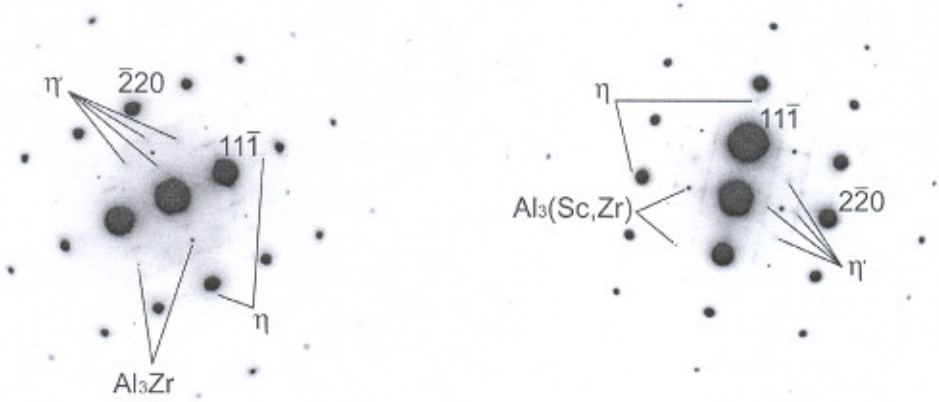

(a) (b)

Figure 9. Selected area diffraction patterns of (a) SSA000 and (b) SSA038 alloy samples after solution annealing, water quenching and subsequent artificial aging at 150°C for 12 hours in $\langle 112 \rangle_{Al}$ projection.

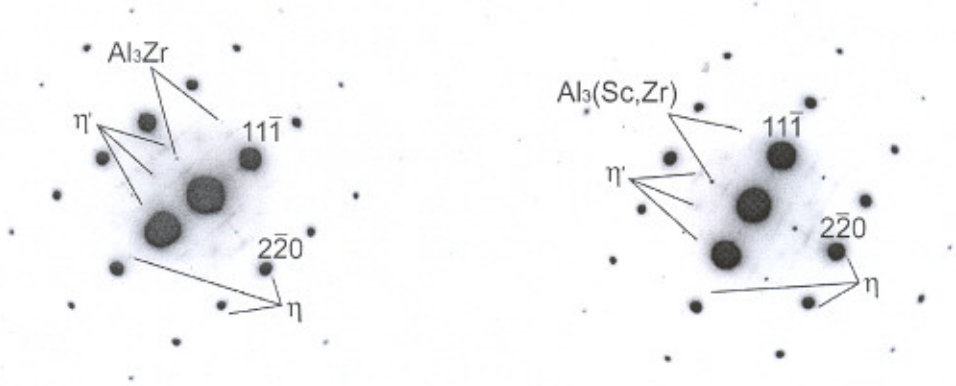

(a) (b)

Figure 10. Selected area diffraction patterns of (a) SSA000 and (b) SSA038 alloy samples after solution annealing, water quenching and subsequent artificial aging at 150°C for 48 hours in $\langle 112 \rangle_{Al}$ projection.

Conclusions

An addition of 0.38 wt.% Sc to a Al-Zn-Mg-Cu alloy results in ~120 MPa increase in the microhardness after solution treatment due to formation of fine coherent $Al_3(Sc,Zr)$ particles.

Kinetics of natural aging of the Sc-containing and Sc-free alloys is essentially the same and is controlled by formation and growth of GPI zones. The difference in the microhardness of these alloys remains unchanging and is the same as after solution treatment (≈120 MPa).

During artificial aging at 120°C, the presence of Sc accelerates formation and growth of GPII zones at the beginning of aging, which results in ~200 MPa higher microhardness value in the SSA038 than in SSA000 after 8 hour aging. However, this accelerated formation and growth of GPII zones in the Sc-

containing alloy leads to coarser η′ and η particles in the peak aged condition and, therefore, reduces the effect of aging on peak microhardness.

The Sc addition does not affect the kinetics of aging at 150°C, which is controlled by formation and growth of η′ and η particles. The difference in the microhardness of these alloys after aging at 150°C is about 80 MPa at any aging time.

Acknowledgements

Help of Dr. R. Wheeler in TEM analysis is greatly appreciated. This work was financially supported through the United States Air Force SBIR Contract No. F04611-02-C-0014 (Mr. Eric Spero, Program Manager).

References

1. J.G. Kaufman (Ed.), Properties of Aluminum Alloys: Tensile, Creep, and Fatigue Data at High and Low Temperatures, ASM International, Materials Park, OH, 1999.
2. J.R. Davis (ED.), Aluminum and Aluminum Alloys, ASM Specialty Handbook, ASM International, Materials Park, OH, 1993.
3. L.K. Berg, J. Gjonnes, V. Hansen, X.Z. Li, M. Knutson-Wedel, G. Waterloo, D. Schryvers, L.R. Wallenberg, Acta Mater., 49 (2001) 3443-3451.
4. G. Sha, A. Cerezo, Acta Mater., 52 (2004) 4503-4516.
5. X.Z. Li, V. Hansen, J. Gjonnes, L.R. Wallenberg, Acta Mater., 47 (1999) 2651-2659.
6. K. Stiller, P.J. Warren, V. Hansen, J. Angenete, J. Gjonnes, Mater. Sci. Eng., A270 (1999) 55-63.
7. A. Deschamps, Y. Brechet, Scripta Mater., 39 (1998) 1517-1522.
8. V.I. Elagin, V.V. Zakharova, T.D. Rostova, Met.Sci. Heat Treatment, 36 (7-8) (1995), 375-380.
9. O.N. Senkov, R.B. Bhat, S.V. Senkova, In: Metallic Materials with High Structural Efficiency, O.N. Senkov, D.B. Miracle, S.A. Firstov, eds., Kluwer Academic Publishers, Dordrecht, The Netherlands, 2004, pp. 151-162.
10. A.F. Norman, K. Hyde, F. Costello, S. Thompson, S. Birley, P.B. Pragnell, Mater. Sci. Eng., A354 (2003) 188-198.
11. O.N. Senkov, R.B. Bhat, S.V. Senkova, J.D. Schloz, Metall. Mater. Trans. A, 36A (2005) 2115-2126.
12. J. Royset, N. Ryum, Internat. Mater. Rev., 50 (2005) 19-44.
13. O.N. Senkov, S.V. Senkova, M.G. Mendiratta, D.B. Miracle, Y.V. Milman, D.V. Lotsko and A.I. Sirko, High Strength Aluminum Alloy Composition, US Patent #7060139, 13 June 2006.
14. O.N. Senkov, S.V. Senkova, M.G. Mendiratta, D.B. Miracle, Method of Making a High Strength Aluminum Alloy Composition, US Patent #7048815, 23 May, 2006.
15. T. Engdahl, V. Hansen, P.J. Warren, K. Stiller, Mater. Sci. Eng., A327 (2002) 59-64.
16. Polmear, Light Alloys: From Traditional Alloys to Nanocrystals, Fourth Edition, Elsevier, Amsterdam, 2006.
17. Y.V.Milman, A.I.Sirko, D.V.Lotsko, D.B.Miracle, and O.N.Senkov, Mater. Sci. Forum, 396-402 (2002) 1217-1222.
18. N. Ryum, Z. Metallkd. 65 (1975) 377-388.
19. R. Howard, N. Bogh, D.S. Mackenzie, in: G.E. Totten and D.S. MacKenzie (Eds.), Handbook of Aluminum, Vol. 1, Physical Metallurgy and Processes, Marcel Dekker, New York, 2003, pp. 881-970.
20. Y. Miura, C. Joh, T. Katsube, Mater. Sci. Forum, 331-337 (2000) 1031-1036.